arXiv:1611.02914v1 [quant-ph] 9 Nov 2016

Engineering thermal reservoirs with ultracold Rydberg atoms

David W. Schönleber, Christopher D. B. Bentley, and Alexander Eisfeld
Max Planck Institute for the Physics of Complex Systems,
Nöthnitzer Strasse 38, 01187 Dresden, Germany

We apply reservoir engineering to construct a thermal environment with controllable temperature in an ultracold atomic Rydberg system. A Boltzmann distribution of the system's eigenstates is produced by optically driving a small environment of ultracold atoms, which is coupled to a photonic continuum through spontaneous emission. This technique provides a useful tool for quantum simulation of both equilibrium dynamics and dynamics coupled to a thermal environment. Additionally, we demonstrate that pure eigenstates, such as Bell states, can be prepared in the Rydberg atomic system using this method.

Introduction.—Solving the dynamics of open quantum systems is one important task addressed by quantum simulators [1–4]. The dynamics generated by the environment-couplings of the target system must be reproduced in the simulator [2, 5]. Coherent [6, 7] and incoherent approaches [8] have been developed for this *reservoir engineering* problem, for particular environments or degrees of freedom in the system. Reservoir engineering [9] involves design of the environment or its coupling to the system, which can be applied in a variety of systems for entanglement generation and protection [10–21], dissipative computation [22] and open quantum system simulation [23–28]. Here, we consider reservoir engineering of an extreme nature: using optical control, we transform a typically non-thermal environment into a thermal environment with controllable temperature. Access to an arbitrary-temperature thermal environment provides two-fold benefits. Firstly, a system with a fixed-temperature environment can simulate more general non-equilibrium dynamics. Secondly, thermal state preparation allows the study of interacting systems initially at equilibrium, which has motivated the design of digital algorithms [29–32].

In this Letter we show that a driven dissipative atomic environment, as shown in Figure 1(a), provides a highly-tunable environment. In our setup, the steady-state populations of the system eigenstates can be precisely controlled by means of currently-achievable frequencies and intensities of the two lasers driving the environment atoms. We prepare system eigenstates and thermal states (i) on a timescale shorter than the system decay timescale and (ii) in a long time limit. While (i) demonstrates dissipative state preparation of entangled and thermal states, (ii) can be used to mimic a thermal environment for a quantum simulator. We highlight that the effective temperature scale of the Boltzmann distribution of eigenstates is determined by the system interaction strength rather than the 'ambient' temperature of the ultracold environment.

Setup.—We consider the setup sketched in Fig. 1(a) and described in detail in the supporting information (SI) and Ref. 33. Dipole-coupled Rydberg atoms constitute

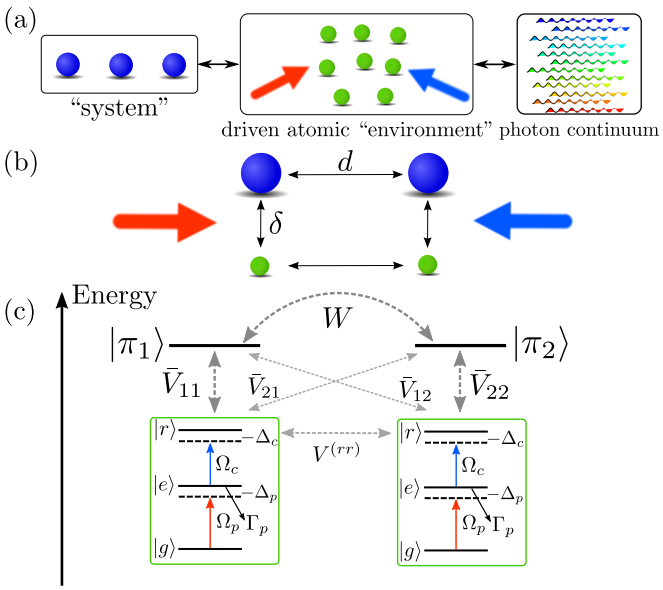

FIG. 1. (Color online) (a) Conceptual sketch of the setup. A "system" of Rydberg atoms is coupled to a laser-driven atomic "environment", which is dissipative through its coupling to the electromagnetic continuum. (b) Implementation. Laser-driven environment atoms are placed at a distance δ from each of the system atoms, which have interatomic separation d. (c) Level sketch. The dimer states $|\pi_1\rangle$ and $|\pi_2\rangle$ (see main text) are coupled to each other via resonant dipole-dipole interaction with strength W and interact with the Rydberg states $|r\rangle$ of the environment atoms via the interactions $\bar{V}_{n\alpha}$. The environment atoms are laser-driven, realizing the level scheme depicted in the green boxes.

our system of interest. Due to their strong interactions and relative ease to laser-control and position experimentally, Rydberg systems have been proposed for quantum simulation of spin Hamiltonians [24, 34], electron-phonon coupling [35], as well as exciton transport [33, 36–40]. The environment for the Rydberg system is provided by laser-driven atoms, which in turn are coupled to a continuum of electromagnetic modes, thereby inducing radiative transitions to lower-energy states (spontaneous emission) in the atomic environment. Interactions between Rydberg system and environment atoms are intro-

duced via Rydberg states of the environment atoms. The tunability of the environment arises through its composition of a finite part, the laser-driven three-level atoms, and an infinite part, the photon bath. By tuning the parameters of the lasers addressing the environment atoms, the timescale of the dynamics within the finite part can be controlled.

We now exemplify the relevant properties of our setup for a Rydberg dimer, i.e., two Rydberg atoms as shown in Fig. 1(b). The atoms are prepared in two different Rydberg states. Here we consider one atom prepared in a Rydberg $|s\rangle = |\nu s\rangle$ state with principal quantum number ν and angular momentum quantum number $\ell = 0$, and the other atom prepared in a Rydberg $|p\rangle = |\nu p\rangle$ state with angular momentum $\ell = 1$. Resonant dipole-dipole interactions of strength W lead to excitation migration [38, 41], described by the Hamiltonian

$$\mathcal{H}_{\rm sys} = W(|ps\rangle\langle sp| + \text{H.c.}) \equiv W(|\pi_1\rangle\langle\pi_2| + \text{H.c.}), \quad (1)$$

where H.c. denotes the Hermitian conjugate and we introduce the notation $|\pi_1\rangle = |ps\rangle$ ($|\pi_2\rangle = |sp\rangle$) to denote the location of the $|p\rangle$ excitation within the system. We will later be concerned with the eigenvalues of this Hamiltonian, given by $E_\pm = \pm W$, and the corresponding Bell eigenstates $|\Psi^\pm\rangle = (|\pi_1\rangle \pm |\pi_2\rangle)/\sqrt{2}$. For simplicity, we do not include the finite lifetime of the system in our calculations; this is approximately 56 μs for the dimer states we consider [42].

The environment for the Rydberg system is provided by laser-driven atoms. For simplicity, we place each at a distance δ from a given system-atom, such that the vectors along d and δ respectively enclose a right angle. The environment atoms are addressed by two laser beams. The first laser, with Rabi frequency Ω_p and detuning Δ_p, couples the ground state $|g\rangle$ of an environment atom to a short-lived intermediate state $|e\rangle$ with radiative decay rate Γ_p. The second laser, with Rabi frequency Ω_c and detuning Δ_c, couples the intermediate state $|e\rangle$ to a Rydberg state $|r\rangle \neq |p\rangle, |s\rangle$.

The Rydberg states $|r\rangle$ of the environment atoms introduce interactions both between the environment atoms and between the environment atoms and system atoms. The environment atoms interact with each other via van der Waals interaction $V^{(rr)}$. The interactions between environment and system atoms are state-dependent,

$$\mathcal{H}_{\rm int} = \sum_{n,\alpha} \bar{V}_{n\alpha} |\pi_n\rangle\langle\pi_n| \left[|r\rangle\langle r|\right]_\alpha, \quad (2)$$

where $\bar{V}_{n\alpha} = V^{(pr)}_{n\alpha} + \sum_{m\neq n} V^{(sr)}_{m\alpha}$ denotes the overall interaction of a specific environment atom α with the entire system if the latter is in the state $|\pi_n\rangle$. Here, $V^{(pr)}_{n\alpha}$ ($V^{(sr)}_{n\alpha}$) indicates the interaction between the $|r\rangle$ state of environment atom α with a $|p\rangle$ ($|s\rangle$) excitation at system atom n. Due to their distance-dependence, the interactions $V^{(pr)}_{n\alpha}$ and $V^{(sr)}_{n\alpha}$ are strongest for $\alpha = n$, i.e. adjacent environment and system atoms.

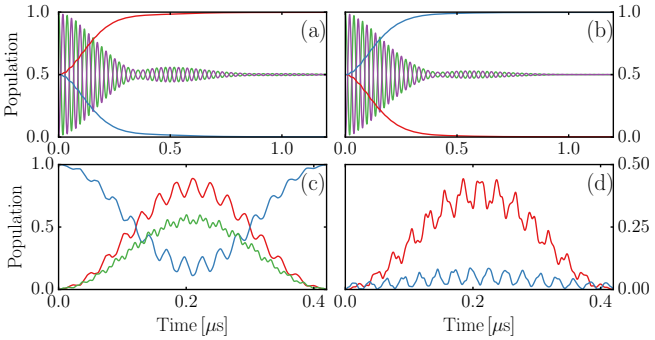

FIG. 2. (Color online) Bell state preparation in a Rydberg dimer. (a,b) Population dynamics of anti-symmetric (a) and symmetric (b) Bell state. Red (blue) lines indicate the population of the anti-symmetric (symmetric) Bell state and green (purple) lines indicate the populations of the states $|\pi_1\rangle$ ($|\pi_2\rangle$). Laser parameters are listed in Tab. 1 in the supporting information (SI). (c,d) Coherent evolution (neglecting dissipation) with parameters as in panel (a). Note the different timescale from the upper plots. In (c), the green (red/blue) line denotes the population dynamics of $P_{r(-/+)}$ after initial preparation in state $|\Psi^+\rangle|gg\rangle$ (cf. main text). (d) The red (blue) line denotes $P_{-(+)}$ as in (c), but additionally projected on the state $|e\rangle$ of the environment.

The resulting level scheme for a Rydberg dimer is shown in Fig. 1(c). For state engineering to be feasible, it is essential that the interaction between an environment Rydberg state $|r\rangle$ and the states $|p\rangle$ and $|s\rangle$ of the adjacent system atom are different, e.g. obeying $|V^{(pr)}_{nn}| \gg |V^{(sr)}_{nn}|$. The numerical values of the interactions are detailed in Ref. 33 and the SI. In the following, we choose the environment-atom geometry such that $d = 5$ μm and $\delta = 2$ μm.

Bell state preparation.—We now show that the Rydberg dimer can be dissipatively prepared in the Bell eigenstates $|\Psi^\pm\rangle$ of the system Hamiltonian, Eq. (1). To this end, we numerically optimize the laser parameters $(\Omega_p, \Delta_p, \Omega_c, \Delta_c)$ for the fixed geometry. Note that the optimized laser parameters are independent of the initial state of system or environment. We thus use a system (environment) state that is easy to access experimentally in our numerical simulations, given by $|\pi_1\rangle$ ($|gg\rangle$).

In Fig. 2 we illustrate the preparation of the anti-symmetric (a) as well as the symmetric (b) Bell state. The marked revival feature in the population dynamics is absent in the dynamics of the eigenstate populations, indicating that the eigenstates can indeed be selectively addressed by the dissipative environment.

To assess the difference between the target density matrix, in this case the projector on the appropriate Bell state, and the density matrix obtained after numerical propagation, we employ two often-adopted distance measures (cf. Refs. 43 and 44). The first measure is the

fidelity $F(\rho_1, \rho_2)$, and the second measure $F_D(\rho_1, \rho_2)$ is related to *trace distance* $D(\rho_1, \rho_2)$ via $F_D(\rho_1, \rho_2) = 1 - D(\rho_1, \rho_2)$. Details are given in the SI [45]. To illustrate the different timescales on which steady-state preparation is feasible, we evaluate the two distance measures F and F_D at $t = 1$ μs and $t \to \infty$ respectively, denoting the $t \to \infty$ case by $\tilde{F}$ and $\tilde{F}_D$. Table 1 in the SI shows that high-fidelity preparation can be achieved on a timescale of about 1 μs.

To gain insight into the dissipative state preparation mechanism, we now examine the underlying coherent evolution for the system and atomic environment. In particular, we consider the preparation of the $|\Psi^-\rangle$ state as in Figure 2(a), while the same mechanism (with $|\Psi^+\rangle \leftrightarrow |\Psi^-\rangle$) describes preparation of the $|\Psi^+\rangle$ state. We accordingly describe the system in terms of its Bell eigenstates, which are separable from environment states containing no Rydberg excitations. In Figure 2(c) we plot the population in a particular Bell state by taking the expectation values of projection operators on the coupled system-environment dynamics (with no dissipative decay from $|e\rangle$),

$$P_{+(-)} = |\Psi^{+(-)}\rangle\langle\Psi^{+(-)}|. \tag{3}$$

The coherent coupling of the $|\Psi^+\rangle$ and $|\Psi^-\rangle$ system states can be seen in the figure, as the $|\Psi^-\rangle$ state becomes accessible through Rydberg-Rydberg interactions between system and environment atoms. When we subsequently project on the environment state $|e\rangle$, we observe the strong correlation in Figure 2(d) between occupation of $|e\rangle$ and the target $|\Psi^-\rangle$ system-state. When decay from $|e\rangle$ is introduced, population is dissipatively pumped into the $|\Psi^-\rangle|gg\rangle$ state, which is effectively dark to both driving and dissipation. Note that the environment atom Rydberg population is shown in Figure 2(c) using the projection operator

$$P_r = \mathbb{1} \otimes |r\rangle\langle r| + |r\rangle\langle r| \otimes \mathbb{1}. \tag{4}$$

The detailed interactions are explored in the SI, as well as detection of the spontaneous decay events, which can herald state preparation and provide conditional enhancement of the state fidelity [20].

Thermal state preparation.—In addition to the preparation of a single system eigenstate, we can also prepare mixtures of eigenstates. To illustrate this, we consider thermal states [46]

$$\rho_T^{\text{th}} = \frac{1}{Z} \sum_n e^{-\mathcal{H}_{\text{sys}}/(kT)} |\varphi_n\rangle\langle\varphi_n|, \tag{5}$$

where $Z = \text{Tr}\{e^{-\mathcal{H}_{\text{sys}}/(kT)} |\varphi_n\rangle\langle\varphi_n|\}$, $|\varphi_n\rangle$ denotes the eigenstates of $\mathcal{H}_{\text{sys}}$, k the Boltzmann constant and T the temperature of the system. Note that the relevant energy scale providing the temperature scale is the resonant dipole-dipole interaction W. For a dimer, the two system eigenstates are separated in energy by $2W$, such that $\rho_T^{\text{th}} \propto (|\varphi_1\rangle\langle\varphi_1| + e^{-2W/(kT)} |\varphi_2\rangle\langle\varphi_2|)$. We emphasize that T is not the ambient temperature of the environment atoms, which is typically $\sim \mu$K. To illustrate the versatility of the scheme we demonstrate low and high temperature mixtures, given by $kT_L = 1.2\ W$ and $kT_H = 12.3\ W$ respectively. The numerical values are chosen such that T_L yields strong asymmetries in the eigenstate populations while T_H yields similar occupations of the eigenstates.

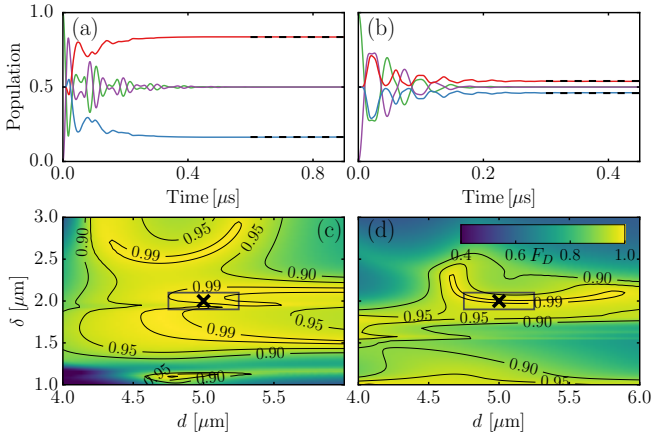

FIG. 3. (Color online) Thermal state preparation in a Rydberg dimer with temperatures T_L (a,c) and T_H (b,d). (a,b) Population dynamics. Solid red (blue) lines denote the population of the lower (higher) energy eigenstate while green (purple) lines indicate localized state $|\pi_1\rangle$ ($|\pi_2\rangle$) population. The target populations are shown with black dashed lines. (c,d) F_D as a function of the dimer separation d and the dimer-environment atom distance δ. Crosses mark the values used in the upper plots. The gray boxes indicate a $\pm 5\%$ uncertainty in the distances. Laser parameters are listed in Tab. 1 in the SI.

For a Rydberg dimer, the preparation of thermal states with temperature T_L (a) and T_H (b) is shown in Fig. 3, using exemplary laser parameter sets. Both states can be prepared with high fidelity (cf. Tab. 1 in the SI).

The thermal state is sustained through competition between the dissipative decay and coherent dynamics. This is in contrast to Bell state preparation, which involves laser parameters such that the target system eigenstate (and ground environment state) is minimally affected by either coherent or incoherent dynamics.

Robustness.—For the target state to be experimentally accessible, it is important that small variations in the laser parameters or distances do not lead to a strong reduction of the fidelity. We have verified this by varying both distances (dimer separation d and dimer-environment atom distance δ) as well as laser parameters. Generally, the laser and distance parameter values required to obtain high target-state fidelities are non-unique, reflecting the grand tunability of our environment. In particular, there are possible parameter varia-

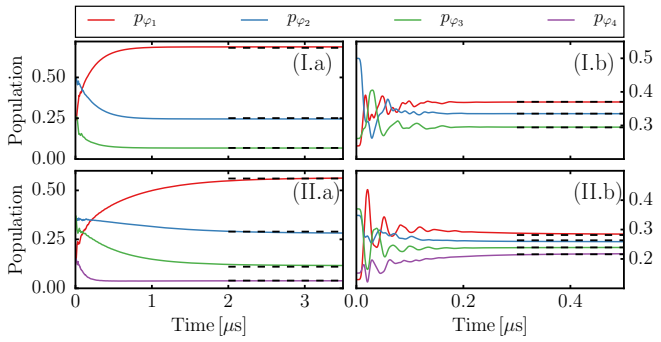

FIG. 4. (Color online) Thermal state preparation in a trimer (I) and quadromer (II) with temperatures T_L (a) and T_H (b). Solid colored lines show the populations p_{φ_n} of the system eigenstates $|\varphi_n\rangle$, and the target populations are indicated with dashed black lines. Laser parameters are listed in Tab. 1 in the SI.

tions around a given parameter set for which the fidelity does not drop significantly. The parameter range for the respective variations depends on the desired target state. To illustrate this, we show in Fig. 3(c) and (d) the dependence of F_D of the two thermal dimer states displayed in Fig. 3(a) and (b) on the distances d and δ. Although the high-fidelity parameter space differs significantly for the two different thermal dimer states, in both cases small variations in the distances d and δ still allow for high-fidelity preparation after a preparation time of $t = 1$ μs.

Results for larger systems.—Dissipative state-preparation is not limited to a Rydberg dimer. In Fig. 4 we demonstrate the preparation of thermal states with temperatures T_L and T_H for a Rydberg trimer ($N = 3$ system atoms) as well as a quadromer ($N = 4$ system atoms) using exemplary laser parameter sets. In both cases, the thermal states can be prepared with high fidelity (cf. Tab. 1 in the SI). However, state-preparation at short timescales becomes more difficult for larger system sizes. In particular, for constant atom spacing, the energy differences between the system eigenenergies decrease with increasing system size. Larger timescales are thus required for distinctive dynamics for individual eigenstates to emerge.

Conclusions and outlook.—We have shown that just a few laser-driven atoms, with global addressing, already realize a tunable environment enabling tailored dissipative state preparation in a Rydberg system. In particular, thermal states with temperatures vastly different from the temperature of the ultracold atomic environment can be prepared with high fidelity, using only the laser frequencies and intensities driving the environment atoms as control parameters. We highlight the flexibility provided by an intermediate, controllable environment for engineering target system-environment interactions; this flexible reservoir engineering is highly desirable for quantum simulation schemes.

We note that scalability of the Rydberg system to larger sizes is limited by the radiative lifetimes of the Rydberg $|p\rangle$ and $|s\rangle$ states. An experimental realization in this case would require conditioning on a non-decayed system. Using higher-lying Rydberg states with longer lifetimes could diminish the demands on the experiment.

SUPPORTING INFORMATION

System and environment Hamiltonian.— We consider a linear chain of N ultracold Rydberg atoms with interatomic spacing d. In this chain, $N-1$ atoms are initially prepared in a Rydberg $|s\rangle = |\nu s\rangle$ state with principal quantum number ν and angular momentum quantum number $\ell = 0$, and the remaining atom is prepared in a $|p\rangle = |\nu p\rangle$ state with $\ell = 1$. The Rydberg states $|s\rangle$ and $|p\rangle$ are coupled via resonant dipole-dipole interactions, resulting in an interaction $W_{nm} = C_3/(d|n-m|)^3$ between states with a localized $|p\rangle$ excitation at atoms n and m, respectively [38, 41]. Ignoring van der Waals corrections [47] and setting the constant energy splitting between $|p\rangle$ and $|s\rangle$ to zero, the Hamiltonian describing the dynamics within the Rydberg system is thus given by

$$\mathcal{H}_{\text{sys}} = \sum_{n\neq m} W_{nm} \, |\pi_n\rangle\langle\pi_m| \,, \tag{6}$$

where we introduce the states $|\pi_n\rangle$ with the $|p\rangle$ excitation localized at atom n, e.g. $|\pi_1\rangle = |pss\cdots\rangle$.

The environment for the Rydberg system is provided by laser-driven atoms, each placed at a distance δ from a given system atom, such that the vectors along d and δ respectively enclose a right angle [cf. Fig. 1(a) in the main text]. The environment atoms are addressed by two laser beams. The first laser with Rabi frequency Ω_p and detuning Δ_p couples the ground state $|g\rangle$ of an environment atom to a short-lived intermediate state $|e\rangle$. The second laser with Rabi frequency Ω_c and detuning Δ_c couples the intermediate state $|e\rangle$ to a Rydberg state $|r\rangle \neq |p\rangle, |s\rangle$. In the rotating wave approximation, the laser Hamiltonian accordingly reads as

$$\begin{aligned}\mathcal{H}_{\text{laser}} = \sum_\alpha \left[\frac{\Omega_p}{2}\left[|e\rangle\langle g|\right]_\alpha + \frac{\Omega_c}{2}\left[|r\rangle\langle e|\right]_\alpha + \text{H.c.}\right] \\ - \Delta_p \left[|e\rangle\langle e|\right]_\alpha - (\Delta_p + \Delta_c)\left[|r\rangle\langle r|\right]_\alpha .\end{aligned} \tag{7}$$

The environment atoms also interact among themselves via Rydberg-Rydberg interaction $V^{(rr)}_{\alpha\beta}$, described by the Hamiltonian

$$\mathcal{H}_{\text{int,env}} = \sum_{\alpha<\beta} V^{(rr)}_{\alpha\beta} \left[|r\rangle\langle r|\right]_\alpha \left[|r\rangle\langle r|\right]_\beta , \tag{8}$$

where α, β label the environment atoms. The total Hamiltonian of the environment is thus $\mathcal{H}_{\text{env}} = \mathcal{H}_{\text{laser}} + \mathcal{H}_{\text{int,env}}$.

The interactions between environment and system atoms are state-dependent,

$$\mathcal{H}_{\rm int} = \sum_{n,\alpha} \bar{V}_{n\alpha} \left|\pi_n\right\rangle\!\left\langle\pi_n\right| \left[\left|r\right\rangle\!\left\langle r\right|\right]_\alpha , \tag{9}$$

where $\bar{V}_{n\alpha} = V^{(pr)}_{n\alpha} + \sum_{m\neq n} V^{(sr)}_{m\alpha}$ denotes the overall interaction of the specific environment atom α with the entire system if the latter is in the state $|\pi_n\rangle$. Note that Latin indices such as n, m refer to system atoms while Greek indices such as α, β to environment atoms. We emphasize that for state engineering, it is essential that the interaction between the $|r\rangle$ state of an environment atom and the $|s\rangle$ and $|p\rangle$ states of an adjacent system atom differ strongly, e.g. obeying $|V^{(pr)}_{nn}| \gg |V^{(sr)}_{nn}|$.

The resulting level scheme for a Rydberg dimer is shown in Fig. 1(c) in the main text, where arrows of different thickness indicate that the dominant interactions between environment atoms and system are *local*, i.e., strongest between the $|p\rangle$ excitation at atom n and the adjacent environment atom n (at a distance δ).

Including spontaneous emission with rate Γ_p from the intermediate state $|e\rangle$ via the Lindblad super-operator

$$\mathcal{L}[\rho(t)] = \sum_\alpha \frac{1}{2} \left\{ [L_\alpha \rho(t), L^\dagger_\alpha] + [L_\alpha, \rho(t) L^\dagger_\alpha] \right\} \tag{10}$$

with Lindblad operator $L_\alpha = \sqrt{\Gamma_p}\left[|g\rangle\!\langle e|\right]_\alpha$, the master equation for the full density matrix ρ of the system and environment takes the form ($\hbar = 1$)

$$\dot{\rho}(t) = -i[\mathcal{H}_{\rm sys} + \mathcal{H}_{\rm env} + \mathcal{H}_{\rm int}, \rho(t)] + \mathcal{L}[\rho(t)]. \tag{11}$$

We now specify our state choice and interactions as in Ref. 33. We take the Rydberg states of the system to be $|p\rangle = |43p\rangle$ and $|s\rangle = |43s\rangle$ of ^{87}Rb, for which $C_3/(2\pi) = 1619$ MHz μm^3. We also consider ^{87}Rb environment atoms, with state choices $|g\rangle = |5s\rangle$, $|e\rangle = |5p\rangle$ and $|r\rangle = |38s\rangle$. The corresponding Rydberg-Rydberg interactions are thus $V^{(rr)}_{\alpha\beta} = C_{6,rr}/(|\alpha - \beta| d)^6$ with dispersion coefficient $C_{6,rr}/(2\pi) = 530$ MHz μm^6, $V^{(pr)}_{n\alpha} = C_{4,pr}/|\boldsymbol{R}_n - \boldsymbol{R}_\alpha|^4$ with dispersion coefficient $C_{4,pr}/(2\pi) = -1032$ MHz μm^4, and $V^{(sr)}_{n\alpha} = C_{6,sr}/|\boldsymbol{R}_n - \boldsymbol{R}_\alpha|^6$ with $C_{4,pr}/(2\pi) = -87$ MHz μm^6.

Distance measures.— Here we detail the two distance measures employed in the main text. The first measure is the *fidelity*. The fidelity between two density matrices ρ_1 and ρ_2 is defined as [43]

$$F(\rho_1, \rho_2) = \mathrm{Tr}\left\{ \sqrt{\sqrt{\rho_1}\rho_2\sqrt{\rho_1}} \right\}, \tag{12}$$

and can be interpreted a generalized measure of the overlap between two quantum states [44].

The second measure is related to the *trace distance* via

$$F_D(\rho_1, \rho_2) = 1 - D(\rho_1, \rho_2). \tag{13}$$

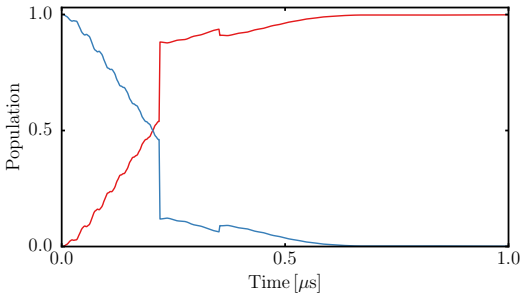

FIG. 5. Stochastic trajectory for $\left|\Psi^-\right\rangle$ state preparation, given perfect detection of emission from the $|e\rangle$ environment state. The red (blue) line shows the $|\Psi^{-(+)}\rangle$ state population. The jump times are at 0.22 μs and 0.35 μs, where sharp features are observed. The system is initially in state $|\Psi^+\rangle\,|gg\rangle$.

The trace distance $D(\rho_1, \rho_2)$, which can be interpreted as a measure of state distinguishability, is defined as

$$D(\rho_1, \rho_2) = \frac{1}{2}\,\mathrm{Tr}\left\{|\rho_1 - \rho_2|\right\}, \tag{14}$$

with $|\rho| = \sqrt{\rho^\dagger \rho}$. From the relation $1 - F(\rho_1, \rho_2) \leq D(\rho_1, \rho_2)$ [43] it follows that $F_D(\rho_1, \rho_2) \leq F(\rho_1, \rho_2)$, which implies that $F_D(\rho_1, \rho_2)$ is a more conservative measure.

Detection.— The stochastic trajectory shown in Fig. 5 corresponds to an unravelling of the master equation (11), with distinguishable detection of the decay events from the environment $|e\rangle$ atomic states. Parameters are chosen for the preparation of the $|\Psi^-\rangle$ state, and are provided in Tab. 1. The population in the $|\Psi^-\rangle$ state increases dramatically at the first jump event, due to the population rescaling according to the $|e\rangle$ populations shown in Figure 2(d) at the appropriate time (see e.g. [48, 49] for a formal treatment of quantum jumps). The subsequent jump then slightly decreases the target state population, which is quickly restored through coherent dynamics. Together, the coherent evolution and spontaneous emission from the $|e\rangle$ state drive the system into the $|\Psi^-\rangle$ state.

This description of the dynamics provides physical insight into the state preparation mechanism, and can even be used to provide conditional enhancement of the state fidelity [20].

Target-state fidelities and parameters.— Table I displays the fidelities and parameters corresponding to the state preparations shown in Figs. 2 to 4 in the main text.

TABLE I. Summary of measures F [Eq. (12)] and F_D [Eq. (13)] as well as the laser parameters $\Omega_p, \Delta_p, \Omega_c, \Delta_c$. The two measures F and F_D are evaluated at $t = 1$ μs (F, F_D) and in the steady state $(\tilde{F}, \tilde{F}_D)$.

N	Target state	$(F, \tilde{F})$	$(F_D, \tilde{F}_D)$	$\Omega_p/(2\pi)$ (MHz)	$\Omega_c/(2\pi)$ (MHz)	$\Delta_p/(2\pi)$ (MHz)	$\Delta_c/(2\pi)$ (MHz)
2	$\left\|\Psi^-\right\rangle\!\left\langle\Psi^-\right\|$	(0.999, 0.999)	(0.992, 0.998)	7.6	95.3	-75.8	-44.9
2	$\left\|\Psi^+\right\rangle\!\left\langle\Psi^+\right\|$	(0.999, 0.999)	(0.997, 0.998)	8.0	89.8	65.3	-7.7
2	$\rho^{\rm th}_{T_L}$	(>0.999, >0.999)	(>0.999, 0.999)	19.7	35.6	-18.1	-4.6
2	$\rho^{\rm th}_{T_H}$	(>0.999, >0.999)	(0.997, 0.997)	30.0	48.9	-7.3	-70.4
3	$\rho^{\rm th}_{T_L}$	(>0.999, >0.999)	(0.994, 0.992)	9.5	34.5	-7.5	-71.0
3	$\rho^{\rm th}_{T_H}$	(>0.999, >0.999)	(0.999, 0.999)	27.8	66.9	-18.3	-33.7
4	$\rho^{\rm th}_{T_L}$	(0.996, >0.999)	(0.931, 0.990)	34.6	34.9	-34.5	-70.6
4	$\rho^{\rm th}_{T_H}$	(>0.999, >0.999)	(0.994, 0.994)	35.0	43.3	-1.3	-45.8

[1] R. P. Feynman, Int. J. Theor. Phys. **21**, 467 (1982).
[2] S. Lloyd, Science **273**, 1073 (1996).
[3] I. Buluta and F. Nori, Science **326**, 108 (2009).
[4] I. M. Georgescu, S. Ashhab, and F. Nori, Rev. Mod. Phys. **86**, 153 (2014).
[5] C. H. Tseng, S. Somaroo, Y. Sharf, E. Knill, R. Laflamme, T. F. Havel, and D. G. Cory, Phys. Rev. A **62**, 032309 (2000).
[6] S. Lloyd and L. Viola, Phys. Rev. A **65**, 010101 (2001).
[7] M. Kliesch, T. Barthel, C. Gogolin, M. Kastoryano, and J. Eisert, Phys. Rev. Lett. **107**, 120501 (2011).
[8] D. Bacon, A. M. Childs, I. L. Chuang, J. Kempe, D. W. Leung, and X. Zhou, Phys. Rev. A **64**, 062302 (2001).
[9] J. F. Poyatos, J. I. Cirac, and P. Zoller, Phys. Rev. Lett. **77**, 4728 (1996).
[10] A. Beige, S. Bose, D. Braun, S. F. Huelga, P. L. Knight, M. B. Plenio, and V. Vedral, J. Mod. Opt. **47**, 2583 (2000).
[11] A. R. R. Carvalho, P. Milman, R. L. de Matos Filho, and L. Davidovich, Phys. Rev. Lett. **86**, 4988 (2001).
[12] B. Kraus, H. P. Büchler, S. Diehl, A. Kantian, A. Micheli, and P. Zoller, Phys. Rev. A **78**, 042307 (2008).
[13] A. R. R. Carvalho, A. J. S. Reid, and J. J. Hope, Phys. Rev. A **78**, 012334 (2008).
[14] H. Krauter, C. A. Muschik, K. Jensen, W. Wasilewski, J. M. Petersen, J. I. Cirac, and E. S. Polzik, Phys. Rev. Lett. **107**, 080503 (2011).
[15] J. Cho, S. Bose, and M. S. Kim, Phys. Rev. Lett. **106**, 020504 (2011).
[16] K. Stannigel, P. Rabl, and P. Zoller, New J. Phys. **14**, 063014 (2012).
[17] Y. Lin, J. P. Gaebler, F. Reiter, T. R. Tan, R. Bowler, A. S. Sørensen, D. Leibfried, and D. J. Wineland, Nature **504**, 415 (2013).
[18] S. Shankar, M. Hatridge, Z. Leghtas, K. M. Sliwa, A. Narla, U. Vool, S. M. Girvin, L. Frunzio, M. Mirrahimi, and M. H. Devoret, Nature **504**, 419 (2013).
[19] F. Reiter, L. Tornberg, G. Johansson, and A. S. Sørensen, Phys. Rev. A **88**, 032317 (2013).
[20] C. D. B. Bentley, A. R. R. Carvalho, D. Kielpinski, and J. J. Hope, Phys. Rev. Lett. **113**, 040501 (2014).
[21] G. Morigi, J. Eschner, C. Cormick, Y. Lin, D. Leibfried, and D. J. Wineland, Phys. Rev. Lett. **115**, 200502 (2015).
[22] F. Verstraete, M. M. Wolf, and J. Ignacio Cirac, Nat Phys **5**, 633 (2009).
[23] S. Diehl, A. Micheli, A. Kantian, B. Kraus, H. P. Buchler, and P. Zoller, Nat Phys **4**, 878 (2008).
[24] H. Weimer, M. Müller, I. Lesanovsky, P. Zoller, and H. P. Büchler, Nature Phys. **6**, 382 (2010).
[25] J. T. Barreiro, M. Muller, P. Schindler, D. Nigg, T. Monz, M. Chwalla, M. Hennrich, C. F. Roos, P. Zoller, and R. Blatt, Nature **470**, 486 (2011).
[26] P. Schindler, M. Müller, D. Nigg, J. T. Barreiro, E. A. Martinez, M. Hennrich, T. Monz, S. Diehl, P. Zoller, and R. Blatt, Nature Physics **9**, 361 (2013).
[27] J. Piilo and S. Maniscalco, Phys. Rev. A **74**, 032303 (2006).
[28] S. Mostame, P. Rebentrost, A. Eisfeld, A. J. Kerman, D. I. Tsomokos, and A. Aspuru-Guzik, New Journal of Physics **14**, 105013 (2012).
[29] B. M. Terhal and D. P. DiVincenzo, Phys. Rev. A **61**, 022301 (2000).
[30] D. Poulin and P. Wocjan, Phys. Rev. Lett. **103**, 220502 (2009).
[31] K. Temme, T. J. Osborne, K. G. Vollbrecht, D. Poulin, and F. Verstraete, Nature **471**, 87 (2011).
[32] M. J. Kastoryano and F. G. S. L. Brandão, Commun. Math. Phys. **344**, 915 (2016).
[33] D. W. Schönleber, A. Eisfeld, M. Genkin, S. Whitlock, and S. Wüster, Phys. Rev. Lett. **114**, 123005 (2015).
[34] I. Lesanovsky, Phys. Rev. Lett. **108**, 105301 (2012).
[35] J. P. Hague and C. MacCormick, New J. Phys. **14**, 033019 (2012).
[36] O. Mülken, A. Blumen, T. Amthor, C. Giese, M. Reetz-Lamour, and M. Weidemüller, Phys. Rev. Lett. **99**, 090601 (2007).
[37] G. Günter, H. Schempp, M. Robert-de Saint-Vincent, V. Gavryusev, S. Helmrich, C. S. Hofmann, S. Whitlock, and M. Weidemüller, Science **342**, 954 (2013).
[38] D. Barredo, H. Labuhn, S. Ravets, T. Lahaye, A. Browaeys, and C. S. Adams, Phys. Rev. Lett. **114**, 113002 (2015).
[39] H. Schempp, G. Günter, S. Wüster, M. Weidemüller, and S. Whitlock, Phys. Rev. Lett. **115**, 093002 (2015).
[40] M. Genkin, D. W. Schönleber, S. Wüster, and A. Eisfeld, J. Phys. B **49**, 134001 (2016).
[41] F. Robicheaux, J. V. Hernández, T. Topçu, and L. D. Noordam, Phys. Rev. A **70**, 042703 (2004).
[42] I. I. Beterov, I. I. Ryabtsev, D. B. Tretyakov, and V. M. Entin, Phys. Rev. A **79**, 052504 (2009).
[43] M. Nielsen and I. Chuang, *Quantum Computation and*

Quantum Information: 10th Anniversary Edition (Cambridge University Press, Cambridge, 2010).
[44] A. Gilchrist, N. K. Langford, and M. A. Nielsen, Phys. Rev. A **71**, 062310 (2005).
[45] See Supplemental Material for details on the Hamiltonian, distance measures of density matrices, and target-state parameters and fidelities.
[46] M.-H. Yung, D. Nagaj, J. D. Whitfield, and A. Aspuru-Guzik, Phys. Rev. A **82**, 060302 (2010).
[47] H. Zoubi, A. Eisfeld, and S. Wüster, Phys. Rev. A **89**, 053426 (2014).
[48] H. Carmichael, *An Open Systems Approach to Quantum Optics* (Springer-Verlag, Berlin, 1993).
[49] K. Mølmer, Y. Castin, and J. Dalibard, JOSA B **10**, 524 (1993).